Water Resources Research

RESEARCH ARTICLE
10.1029/2020WR029321

Assessing the Effects of Climate Change on Compound Flooding in Coastal River Areas

M. Bermúdez[1], J. F. Farfán[2], P. Willems[3], and L. Cea[2]

[1]Environmental Fluid Dynamics Group, Andalusian Institute for Earth System Research, University of Granada, Granada, Spain, [2]Water and Environmental Engineering Group, Department of Civil Engineering, Universidade da Coruña, A Coruña, Spain, [3]Department of Civil Engineering—Hydraulics Section, KU Leuven, Leuven, Belgium

Key Points:

- A continuous simulation approach is used to evaluate the impact of climate change in compound flooding from river discharge and sea level
- Local-scale physically consistent projections are obtained in order to account for climate change effects on the flood drivers
- Our results show the substantial role of both the sea level rise and the increases in maximum river discharges in future flood hazard

Supporting Information:

Supporting Information may be found in the online version of this article.

Correspondence to:

M. Bermúdez,
mariabermudez@ugr.es

Citation:

Bermúdez, M., Farfán, J. F., Willems, P., & Cea, L. (2021). Assessing the effects of climate change on compound flooding in coastal river areas. *Water Resources Research*, *57*, e2020WR029321. https://doi.org/10.1029/2020WR029321

Received 25 NOV 2020
Accepted 4 OCT 2021

Abstract Flood assessment in coastal river areas is subject to complex dependencies and interactions between flood drivers. In addition, coastal areas are especially vulnerable to climate change, and thus its effects should be considered in the evaluation of future flood hazard. In the present study, we propose a methodology for a robust evaluation of historical and future flooding in coastal river areas. It follows a continuous simulation approach in which a hydrologic-hydraulic modeling cascade is run for several years, driven by a simultaneous series of flood drivers. The method differs from other existing methodologies in: (a) jointly considering the relevant flood drivers, both coastal and inland, together with their dependencies and interactions, to represent the simultaneous occurrence of extreme water levels correctly, and (b) obtaining local-scale physically consistent projections of flood drivers to account for future climate change effects on compound flood hazard. The methodology is tested for a coastal river reach in NW Spain. The results show that, although mean sea level rise is usually expected to be the main driver of increased flood hazard, climate change effects on river discharge can play a very significant role in regions with compound flooding potential.

1. Introduction

Globally, floods are the most common natural hazard and have major economic, social, and ecological impacts on communities (CRED & UNISDR, 2015). Coastal river areas concentrate population, infrastructure, and economic activity, all of these highly vulnerable to floods (Koks et al., 2015). The effects of global warming in such already flood-prone areas raise concerns about future flood conditions, making imperative the need for reliable methods for their analysis (Seneviratne et al., 2012) and innovative approaches to their planning and management.

These challenges, however, have been insufficiently addressed by regulations and policies. In the European Union (EU), the EU Floods Directive (2007/60/CE) and the Water Framework Directive (2000/60/EC) establish the framework for assessing and managing flood risks. It defines a cycle that includes a preliminary assessment to identify areas at risk of flooding, the creation of flood hazard and risk maps, and the establishment of flood risk management plans focused on prevention, protection, and preparedness. It also establishes that these steps need to be reviewed every 6 years, and acknowledges the need to take into account the likely impact of climate change on the magnitude and frequency of floods. The European Water Framework Directive does not go beyond these procedural obligations, leaving open the question as to which methodological approaches are most appropriate for such flood risk assessments.

The prediction of flooding in coastal river areas is not an easy task due to the complexity and interaction of the underlying physical processes. Elevated water levels in coastal reaches originate from the interaction of several coastal and inland drivers, such as storm surge and river discharge. These flood drivers are often not independent since they share a common meteorological forcing. For example, the combined effects of low atmospheric pressure and strong winds associated with synoptic-scale storms can induce storm surges along the coast. Concurrently, or in close succession, heavy precipitation increases freshwater runoff, and as a result leads to high river discharge. Elevated sea levels can block or slow down river drainage into the sea, leading to increased upstream water levels. Compared to flood events caused by a single driver, compound floods can usually be expected to yield higher impacts, as evidenced, for example, in the recent floods in Ravenna (Italy) (Bevacqua et al., 2017) or in the Hurricane Harvey Flood in Houston Area (Valle-Levinson

et al., 2020). In fact, many recent studies have underlined the importance of considering the dependencies and interactions of drivers when assessing flood risk (Bevacqua et al., 2019, 2020; Couasnon et al., 2020; Hendry et al., 2019; Paprotny et al., 2020; Ward et al., 2018). For further details on the drivers of compound flooding events, the reader is referred to the above studies.

Adding the effects of global warming to compound flood hazard involves obtaining future projections of the different flood drivers in a physically consistent way. Mean sea-level rise (SLR) is one of the best-established consequences of global warming, which directly impacts the risk of coastal flooding. It implies not only an increase in the level of permanent inundation (i.e., the area underwater at high tide), but also a larger flood extent in areas far from the coast, since the tide can propagate further upstream the river (Ensign & Noe, 2018; Ganguli & Merz, 2019). As a result, water level exceedances above flooding thresholds, such as the nuisance flood levels established by NOAA's National Weather Service at U.S. tide gauges, are increasing in time (Sweet & Park, 2014). Projections of extreme water levels also suggest that today's century level floods might become decadal by 2050 (Tebaldi et al., 2012).

Although the observed increase in extreme high water levels in coastal areas has been attributed largely to the SLR (Menéndez & Woodworth, 2010), changes in storminess itself can also play a role in future extreme water levels (Vousdoukas et al., 2017). This is the case in regions where flood hazard is driven not only by sea levels but also by inland drivers such as precipitation, which will likely undergo a variety of changes in extreme values (Tabari, 2020). Global climate model (GCM) projections are typically used to quantify future changes in atmospheric variables and run local flood inundation models. But methodologies are far from straightforward, given the mismatch between the spatial and temporal scales of the GCM output and those needed to drive local flood inundation models (van den Hurk et al., 2018). Downscaling techniques, either statistical or dynamical, are typically used to obtain higher resolution climatic projections (Fowler et al., 2007; Maraun et al., 2010). For a review of the skills and limitations of different downscaling methods, see (Ekström et al., 2015).

In the present study, we propose a new methodology for a robust assessment of compound flooding in coastal river areas, considering the effects of future climate change on rainfall and river discharge, storm surge, and mean sea level. The method differs from other existing methodologies in: (a) using a continuous simulation approach that considers the dependencies and interactions of the most relevant flood drivers, in order to represent the simultaneous occurrence of extreme water levels correctly, and (b) obtaining local-scale physically consistent projections of flood drivers to account for future climate change effects on compound flood hazard. Future changes in river morphology and land uses in the floodplains are not considered. The study is limited to the effect of climate change in atmospheric patterns, assuming that their impact on river morphology is negligible. The methodology is tested in a coastal river reach located in NW Spain. The river reach flows through a consolidated urban area with a well-established river encroachment, and hence only small changes in the river morphology are expected to occur during this century.

2. Study Site

The mouth of the river Mandeo, which flows into the estuary of Betanzos (NW Spain), has been used as the study site to show the application of the proposed methodology (Figure 1). Due to the industrialization and urbanization of the floodplains in recent decades, as well as the construction of a train embankment that crosses the estuary, this river reach suffers from recurrent flooding, especially when high tidal ranges occur simultaneously with high river discharges. The confluence between the river Mandeo and its tributary Mendo is located just before the mouth, and it is included in the study area.

The catchment area of the rivers Mandeo and Mendo is 450 km^2, of which 350 km^2 correspond to the Mandeo basin and 100 km^2 to the Mendo basin. The average annual rainfall in both catchments is about 1,250 mm, while the average maximum annual discharges are of the order of 200 and 20 m^3/s respectively in the Mandeo and Mendo rivers (Cea & Fraga, 2018; Sopelana et al., 2018).

The spring tidal range in the estuary of Betanzos is about 4.5 m, and is therefore a macrotidal coastal area according to the classification proposed by Davies (1964), which defines macrotides as those with a tidal range greater than 4 m. Moreover, due to the bathymetry of the estuary, the tidal range has a significant

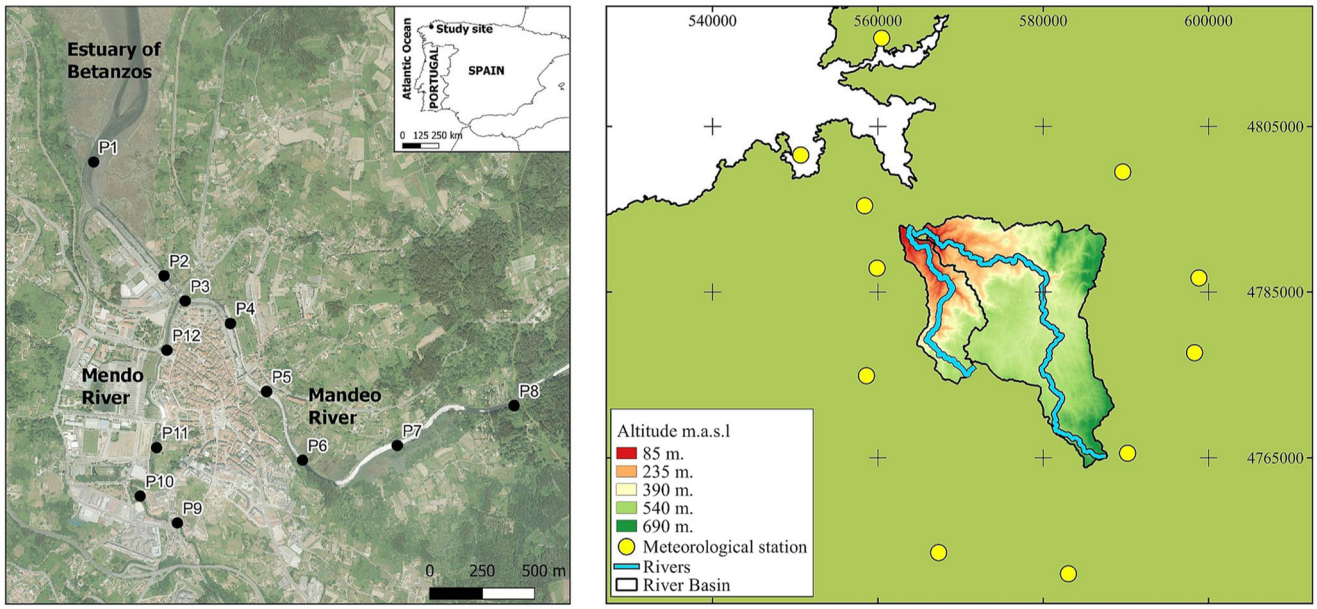

Figure 1. (Left) Location of the study site and aerial image of the study area showing the town of Betanzos and the control points along the rivers Mandeo and Mendo. (Right) Study catchments and location of the 11 meteorological stations used to estimate the rainfall and temperature time series for the whole catchments.

effect on inundation levels. On the other hand, the maximum values of storm surge registered in the estuary are roughly 40 cm and have a lower effect on flooding than the astronomical tide (Bermúdez, Cea, & Sopelana, 2019). In fact, the Northwest region of Spain, where the estuary is located, has been classified by Rueda et al. (2017) as a macrolevel tide-dominant region, with an average relative contribution of the astronomical tide to the annual maxima of sea level above 80%.

Twelve control points distributed along the Mandeo and Mendo rivers were chosen for a detailed analysis of the results (Figure 1). Depending on their distance to the mouth, the relevance of sea level and river discharge on the water depth during a flood varies from one control point to another. Control points 1 to 3 are located downstream of the confluence of both rivers. Control points 4 to 8 are located in the Mandeo river (control point 8 being located more upstream). Control points 9 to 12 are located in the Mendo river (control point 9 being the nearest to the upstream boundary).

3. Methodology

3.1. General Description of the Methodology

The procedure used for obtaining future projections of water depths in a coastal river reach is schematically depicted in Figure 2. The methodology is based on the future projections of temperature, rainfall, sea level pressure, wind and sea-level rise given by GCMs. Together with the tidal range, which is a deterministic variable that is not affected by climate change, these variables are considered to be the main atmospheric and oceanographic drivers of floods in coastal river reaches. Since GCMs only provide projections of these variables at a coarse spatial and temporal resolution (typically in the order of 100 km and 1 day), a weather-typing based statistical downscaling method is applied to produce local projections of rainfall from the large-scale values of temperature, rainfall and sea-level pressure. Regression-based statistical downscaling is also used to transform the large-scale sea level pressure and wind values into local values of storm surge. The downscaling techniques applied are further described in Section 3.3 and 3.4.

The downscaled time series of rainfall and temperature are then fed into a hydrological model to obtain local-scale projections of river discharge. The description of the hydrological model used, and its calibration, is included in Section 3.6.

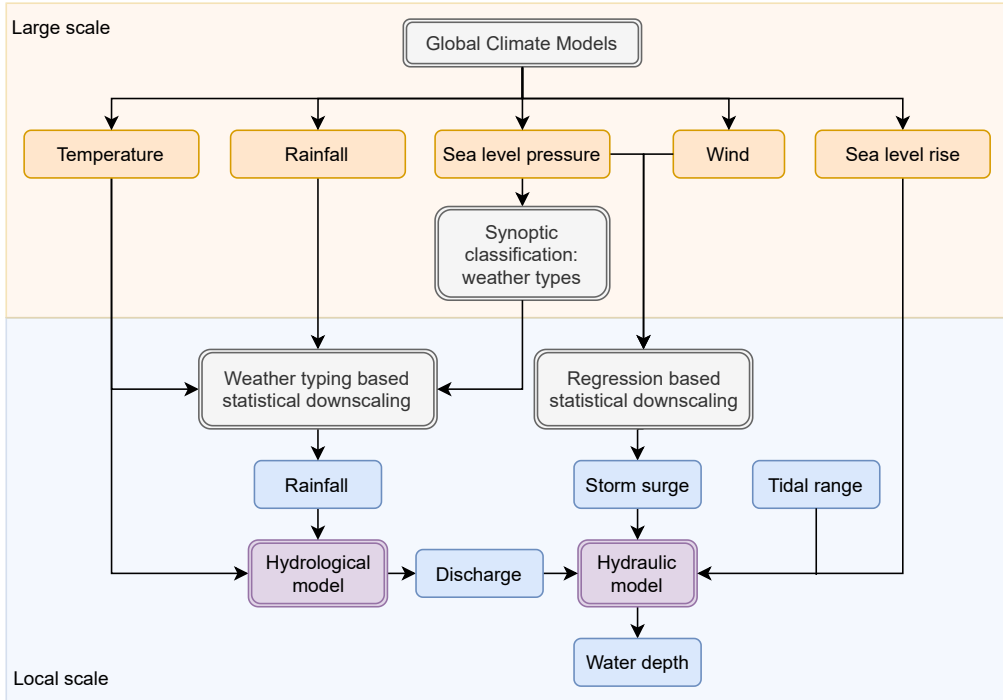

Figure 2. Flow diagram of the proposed methodology to obtain time series of maximum daily water levels in the study area for future RCP scenarios.

The downscaled river discharge and storm surge time series, together with the projected sea-level rise and the deterministic astronomical tidal range, are then used as external forcings in a 2D flood model to obtain time series of water depth at the river reach scale. This is done by means of the continuous simulation approach presented in Sopelana et al. (2018). This approach consists of running a flood inundation (hydraulic) model over a long period of time (several years) driven by simultaneous time series of the flood drivers, in order to reconstruct the time series of maximum daily water depth in the study area. By using simultaneous time series of the flood drivers, the method implicitly considers their statistical dependence.

The main differences between the implementation used in this research and the original study by Sopelana et al. (2018) lie in the flood drivers considered, as well as in the generation of the time series of river discharge and storm surge. In the present study, we have incorporated the mean sea level rise as an additional driver in order to account for global warming in future scenarios, which was not included in the original methodology. At the same time, we have not considered the influence of the time lag between peak discharge and high tide, because in this river reach the high part of the flood hydrographs is maintained for several hours, with discharges similar in magnitude to the peak discharge. Thus, during a typical flood, the discharge at the time of high tide is in general very similar to the peak discharge. Moreover, not considering the time lag between the peak river discharge and high tide in the analysis of compound flooding on this site is justified if we look at the findings of Bermúdez, Cea, and Sopelana (2019), who concluded that the effect on the inundation levels of the timing between maximum river discharge and high tide was close to zero in this catchment.

Regarding the generation of the time series of discharge, Sopelana et al. (2018) used for this purpose a regression regional hydrological model based on the mean annual precipitation, catchment area, mean catchment slope and mean SCS curve number, which was calibrated using observed discharge data at 18 gauge stations located in the hydrological region where the study site is located. Instead of doing that, we have used the hydrological model described in Section 3.6 in order to transform the downscaled time series of precipitation and temperature into discharge time series. This procedure allows us to consider the effect of climate change on river discharge through the projections of precipitation and temperature given by GCMs.

On the other hand, the approach used in Sopelana et al. (2018) to generate the discharge time series cannot be used to evaluate the effect of climate change, since it is based entirely on observed historical discharges.

Regarding the time series of storm surge, these have been generated using a linear regression with the inverted sea level pressure (SLP) given by the GCMs for the future period, as detailed in Section 3.4. This allows us to account for the effect of future climate changes on SLP, as well as for the seasonality and correlation between river discharge and storm surge, since the projected time series of rainfall and SLP are obtained from the same GCMs, and thus they are physically correlated. On the other hand, the procedure followed in Sopelana et al. (2018) to generate the surge time series was based wholly on the observed mean and standard deviation of the daily surge, and hence it cannot be used to evaluate the effects of climate change.

Consequently, the methodology applied in the current study accounts for the joint probability of occurrence of different sources of flooding and their mutual interaction, as well as the seasonal variability of the variables involved.

In order to evaluate changes in flood hazard due to climate change, the above methodology was applied not only to the future period (2071–2100), but also to a historical period (2001–2017). The only difference in applying the method to the two periods is the way in which the time series of the flood drivers were obtained. In Section 3.2, we describe the sources and the methodology used to obtain continuous time series of the large-scale variables in both periods. We then explain the procedure used to estimate local-scale projections of rainfall (Section 3.3), storm surge (Section 3.4), and astronomical tidal range (Section 3.5). The description of the hydrological model used to obtain the time series of discharge is described in Section 3.6. The hydraulic model that provides water levels in the study area is described in Section 3.7.

3.2. Large-Scale Flood Drivers

Temperature, rainfall and sea level pressure time series were obtained from an ensemble set of GCM climate projections, comprising 19 GCMs and 2 RCPs (4.5 and 8.5), in the grid cell containing the catchment centroid, with a time resolution of 1 day. Additional variables can be incorporated in the methodology in cases where other flood drivers have an influence on inundation levels. This is the case with wind, which appears in Figure 2 for the sake of generality, but has little influence on the storm surge levels in the studied area, as shown in Section 3.4.

Mean SLR time series for the study area, relative to the average sea level in the period 1986–2005, were obtained from the Fifth Assessment Report of the Intergovernmental Panel on Climate Change (IPCC-AR5) through the Integrated Climate Data Center website hosted at the University of Hamburg. The time series of mean sea level rise for RCP8.5 and RCP4.5 obtained from the ensemble of GCMs were used in this study (Figure S4 in Supporting Information S1).

For the historical period, temperature time series in the study catchment were generated by combining the observations of 11 meteorological stations located around the rivers Mandeo and Mendo (Figure 1), and operated by the regional meteorological agency Meteogalicia (Table 1). The temperature at the centroids of the catchments was estimated from the hourly temperature data registered at these stations, using an inverse distance interpolation. Daily SLP observations for the historical period were obtained from a buoy close to the studied area (Table 1).

3.3. Weather Typing-Based Statistical Downscaling of Rainfall

The weather typing-based statistical downscaling method SD-B-7 (Willems & Vrac, 2011) was used to downscale rainfall from the ensemble set of 38 GCM climate projections. Compared to other downscaling methods, it has the advantage of being computationally efficient to use with multi-model projections while yielding physically interpretable links between the large-scale circulation and local precipitation. The method relies primarily on the simulated large-scale atmospheric circulation to obtain future precipitation series. The ability of the selected GCMs to reproduce the large-scale atmospheric circulation in this area was verified in Bermúdez et al. (2020), by comparing the WT classification obtained from the control runs of the GCMs (1961–1990 period) and that obtained from the ERA-Interim data set.

Table 1
Input Data and Sources

Variable	Type	Time resolution	Period	Source	Aim
Precipitation	Observations	10 min	2008–2016	Meteo stations of MeteoGalicia[a]	Calibration and validation of hydrological model
			2001–2017	Meteo stations of MeteoGalicia[a]	Computation of historical discharge series / WT-based rainfall downscaling
	Models	1 day	2071–2100	CMIP5 (19 models, 2 RCPs)[b]	WT-based rainfall downscaling
Temperature	Observations	1 hr	2008–2016	Meteo stations of MeteoGalicia[a]	Calibration and validation of hydrological model
			2001–2017	Meteo stations of MeteoGalicia[a]	Historical discharge series / WT-based rainfall downscaling
	Models	1 day	2071–2100	CMIP5 (19 models, 2 RCPs)[b]	WT-based rainfall downscaling
Sea level pressure	Observations	1 day	1998–2017	Buoy Vilano-Sisargas REDEXT network[c]	Computation of historical surge series / Surge downscaling
	Models	1 day	1979–2015	ECMWF-Era Interim[d]	WT-based rainfall downscaling
			2071–2100	CMIP5 (19 models, 2 RCPs)[b]	WT-based rainfall downscaling / Surge downscaling
Storm surge	Observations	1 day	1998–2017	Tidal gage A Coruña—REDMAR network[c]	Computation of historical surge series / Surge downscaling
Sea level rise	Models	1 year	2071–2100	IPCC-AR5 (ICDC—Hamburg University)[e]	Future SLR series
Tidal constituents	Observations	–	–	Tidal gage A Coruña—REDMAR network[c]	Historical and future tidal range series
Discharge	Observations	1 hr	2008–2016	Stream gauges of Augas de Galicia[f]	Calibration and validation of hydrological model

[a]Galician Meteorological Agency: http://www.meteogalicia.gal/observacion. [b]Coupled Model Intercomparison Project Phase 5. [c]Puertos del Estado: http://www.puertos.es/es-es/oceanografia/. [d]European Centre for Medium-Range Weather Forecasts: https://www.ecmwf.int. [e]Integrated Climate Data Center: http://icdc.cen.uni-hamburg.de/. [f]Galician Water Administration: https://augasdegalicia.xunta.gal/.

The downscaling method is described in detail in Willems and Vrac (2011), and thus only a brief explanation is given in the following. First, the large-scale atmospheric circulation affecting the study area was classified into 10 weather types (WTs) based on the Jenkinson Collison system (Jenkinson & Collison, 1977), as explained in Bermúdez et al. (2020). Daily mean SLP from the ERA-Interim dataset and SLP projections from the set of GCMs were the input for this classification step (Table 1) in the historical and future periods, respectively. Second, daily rainfall time series were taken from the GCM grid cell containing the catchment centroid. For each day in the future scenario period (2071–2100), the WT, the season and the exceedance probability of the daily precipitation amount were used to identify analogue days from the historical series. The exceedance probability was computed after sorting all daily precipitation values for that season and WT, and calculating the empirical exceedance probability for each of these daily precipitation values. The latter was done for both the historical data and the GCM data. The analogue day was selected as the day where the exceedance probability of the daily precipitation value for the historical period was closest to the exceedance probability of the daily precipitation value in the GCM data (for the same season and WT). The method did not involve bias correction as it uses the high-resolution data from the analogue day in the past, which is based on real (so no biased) observations. The projected downscaled precipitation time series at 10-minute resolution were constructed by combining the precipitation amount sequences for the analogue

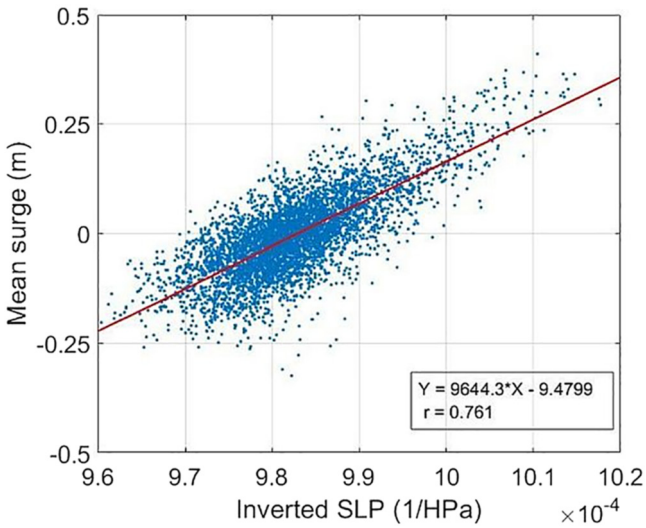

Figure 3. Inverted sea-level pressure (1/HPa) versus mean storm surge (m) for the period 1998–2017.

days. Finally, they were rescaled following the Clausius-Clapeyron relation, which assumes an intensification of extreme precipitation amounts by 7% per degree temperature increase. The variable considered in this step was the temperature rise from the control to the scenario period and not the direct GCM temperature results. Therefore, the future precipitation time series are not affected by potential biases in the GCM temperature simulations (assuming, of course, that any climate model biases are time-invariant).

Historical rainfall time series in the study catchment were generated by combining the observations of the 11 meteorological stations of Meteogalicia shown in Figure 1 (Table 1). The rainfall data registered by the pluviometers were spatially interpolated with a spatial resolution of 1 km and a time resolution of 10 minutes, using a natural neighbor interpolation, and then averaged over the whole catchment to obtain a basin-averaged time series of rainfall that was used in the hydrological model.

3.4. Regression-Based Statistical Downscaling of Storm Surge

A regression-based statistical downscaling method was used to obtain storm surge projections from the set of GCMs. To do so, an empirical relationship between surge, atmospheric pressure and wind was sought using observed data from these variables in the period 1998–2017. The comparison between surge, wind and sea level pressure records showed that storm surge in the studied area is driven mostly by SLP (Figure 3), which can be explained by the narrow continental shelf of the Spanish Atlantic coast. No significant correlation between surge and wind was found. Daily SLP observations, obtained from a buoy close to the studied area, were thus used to establish the relationship with the storm surge. A linear regression was used to compute the mean daily storm surge, with the inverted SLP series representing the independent variable. The Pearson coefficient for the period 1998–2017 was 0.761 (Figure 3). This regression was applied to the future period, using the SLP projections of the set of GCMs (Table 1).

Storm surge observations for the historical period were obtained from a tidal gauge located near the mouth of the river (Table 1).

3.5. Astronomical Tidal Range

The astronomical tide is a deterministic process; therefore, the tidal range time series was generated from the tidal harmonic constituents at the study site, these obtained from historical records of sea level measured at a tidal gauge located in the outer estuary (Pérez Gómez & Begoña, 2014) (Table 1). Since the astronomical factors that cause the tides are not affected by climate change, the same tidal constituents were used for the historical and future scenarios. The tidal dynamics can, however, be altered by non-astronomical factors such as increases in water depth due to SLR or variations in stratification due to increased surface water temperatures (Devlin et al., 2017). The modeling study of Pickering et al. (2017) projects a slight decrease in the M2 amplitude (~2 cm) around the study area in response to a 2 m SLR. Tide gauge analysis also shows a downward trend in tidal amplitude of 0.6 mm/y between 2000 and 2015 (Serrano et al., 2020). Based on the above, the changes in tidal range are expected to be two orders of magnitude lower than the SLR at this location, and have been neglected in this study.

3.6. Hydrological Modeling

A hydrological model was used to transform rainfall and temperature time series into discharge time series. The model used was an adaptation of the Modello Idrologico SemiDistribuito in continuo (MISDc) (Camici et al., 2011). The original version of this model was designed to simulate flood events by coupling a soil water content model with an event-based hydrological model. The soil moisture is computed continuously and used to estimate the initial soil moisture conditions before a flood event. The adaptation of the model used

Table 2
Description of the Physically Based Parameters of the Hydrological Model, From Camici et al. (2011)

Description	Units	Range
Maximum water capacity of the soil layer	mm	100–1000
Pore size distribution index	–	0.05–0.5
Saturated hydraulic conductivity	mm/hr	1.1–20.0
Baseflow to drainage ratio	–	0.1–1.0
Lag-area parameter	–	0.5–6.5
Correction factor for evapotranspiration	–	0.4–2.0
Coefficient to compute soil max retention from soil water content	–	1.0–4.0

in this study implements a baseflow component by introducing a power function that relates the soil moisture to the baseflow, as proposed in Brocca et al. (2013). Detailed descriptions of the model are available in Brocca et al. (2013) and Camici et al. (2011). The application of the model requires rainfall and temperature time series with an hourly resolution as input data to compute the discharge time series at the basin outlet. The model has seven physically based parameters that need to be calibrated with observed data (Table 2). The typical range of variation of these parameters is also shown in Table 2.

The physically based hydrological model was applied within an ensemble model approach. Ensemble modeling consists of selecting the results of a number of different model simulations and combining them to reduce model uncertainties in the discharge predictions (Andraos & Najem, 2020). An ensemble approach might be built by using the results obtained from the same hydrological model and different parameter sets (single-model ensemble) or by combining the results obtained from different hydrological models (multi-model ensemble). Several methods to combine the results of the different model runs have been proposed, including the arithmetic average, the weighted average, multiple linear regression approaches, and soft computing techniques such as artificial neural networks (ANNs) (Kumar et al., 2015; Viney et al., 2009). As a result, a new ensemble hydrograph is obtained, in which the deficiencies of each model run are compensated for by the other model runs in the ensemble (Li & Sankarasubramanian, 2012). In this way, the ensemble hydrograph is more accurate than the hydrographs obtained by each model run.

In this study, we built a single-model ensemble by using the hydrographs computed with different parameter sets of the MISDc model (Table 2). The MISDc hydrographs were used as the input of an ANN, in order to combine them into a single hydrograph. The ANN used to combine the MISDc hydrographs had one hidden layer with three neurons and the hyperbolic tangent as transfer function. The ANN was trained using the Bayesian Regularization algorithm. First, the hydrological model was run in the calibration period (from October 2008 to September 2013) with 5,000 different combinations of the parameters shown in Table 2, these randomly generated using the Latin Hypercube Sampling technique. From the results of these 5,000 model runs, a small number of output hydrographs (those with the highest Pearson coefficient when compared against field observations) were selected in order to build the single-model ensemble. The number of hydrographs used as input for the ANN was 10 in the Mandeo basin and 15 in the Mendo basin (this number was found after a trial and error process). The ANN was trained with observed data in the calibration period, and then the whole ensemble model was validated in the period from October 2013 to September 2016 (validation period). A more detailed description of the single-model ensemble technique is provided in Viney et al. (2009) and Gourley and Vieux (2006), and is not detailed here for the sake of conciseness. More details about the application of ANN to ensemble modeling can be found in Andraos and Najem (2020); Farfán et al. (2020); Li et al. (2018).

Once the model was calibrated and validated, it was applied to reconstruct the discharge series for the period 2001–2017 with a time resolution of 1 hr, using the precipitation and temperature information for this period as input data. For the future scenarios, the downscaled projected precipitation time series and temperature projections of GCMs were used to obtain the projected time series of discharge for each GCM and RCP considered. No downscaling was applied to the time series of temperature since those were only used to evaluate the daily rate of potential evapotranspiration. They thus play a less relevant role than

the precipitation series in driving the model output, and the spatial and temporal resolution provided by the GCMs is enough. It is also worth noting that the potential evapotranspiration is computed from daily average temperature values (not sub-daily extremes), which are usually well-represented in CMIP5 GCMs (Sillmann et al., 2013), and that we are using a multi-model ensemble of GCMs which can compensate deficiencies of individual models (Pierce et al., 2009). However, it would also have been possible to apply a separate bias correction method to improve the GCMs' skill in simulating daily mean temperature.

3.7. Hydraulic Modeling

The two-dimensional shallow water equation model Iber+ (Bladé et al., 2014; García-Feal et al., 2018) was used to compute the spatial distribution and temporal evolution of water levels in the study area. The Iber model has been validated extensively and applied to a number of river inundation studies, showing its ability to represent 2D free surface shallow flows and river inundation processes, and to deal efficiently with some of the main numerical difficulties that arise in the modeling of overland flow, such as the presence of highly unsteady wet-dry fronts, small water depths, and high bed friction (Areu-Rangel et al., 2019; Bermúdez et al., 2017; Cea & French, 2012; Sopelana et al., 2018). The performance of the hydraulic model was not validated in the study area because insufficient historical water depth data were available. Nevertheless, the model solves the full 2D shallow water equations on a high-resolution grid (up to 1 m resolution in areas with large elevation gradients), using very detailed LIDAR data (1 m resolution). In this way, small-scale structural elements (e.g., buildings, walls) and small topographic variations are explicitly represented and not parameterized. The only model parameter is the Manning roughness coefficient, which is set to represent only small-scale roughness, its calibration being less important than for low spatial resolution models. Plausible values were established from River Engineering Manuals, considering the land uses in the study area. A sensitivity analysis of the simulated water levels to Manning's values was also conducted to verify that the uncertainty in the results due to a lack of field calibration is low. Based on the above, the model is considered to provide high fidelity hydraulic simulations of the inundation process in this area for the purposes of this work. For a detailed description of the model's configuration for this river reach, see Bermúdez et al. (2020).

The hydraulic modeling was implemented within the continuous simulation framework proposed in Sopelana et al. (2018) for the estimation of compound inundation in coastal river reaches. The steps of the method were as follows: (a) generate time series of the relevant flood drivers in the study site for a period of several years at a daily scale (these series must be concurrent and must reflect the seasonality and correlations between predictors, in order to represent the simultaneous or closely successive occurrence of extreme values correctly); (b) convert the time series of the flood drivers to time series of maximum daily water depth at relevant control points located within the study site; (c) perform a statistical analysis of the reconstructed water depth time series in order to obtain the desired extreme value estimators.

The generation of the time series of the local flood drivers (river discharge, storm surge, astronomical tide, and mean sea level) from the GCMs large scale projections has already been explained in the previous sections. The flood drivers at the daily scale considered in the continuous simulation approach are the astronomical tidal range (TR), the daily mean storm surge (S), the daily peak discharge (Q), and the mean SLR. Figure S3 in Supporting Information S1 shows an example of the time series that are generated following this methodology.

Following the framework proposed in Sopelana et al. (2018), the hydraulic inundation modeling was done on a daily basis, that is, one model run for each day in the time series. This is justified because flood events in this reach last between 12 and 24 hr. The boundary conditions for each model run were defined from the daily flood drivers. In order to do so, the astronomical tide and the river discharge were further downscaled to a time resolution of 15 min, as explained in (Sopelana et al., 2018). On the other hand, the storm surge and the sea level rise were assumed to be constant during each day, and thus the sum of both values was imposed as an offset elevation to be added to the astronomical tide time series. The storm surge in this coastal region is generated by low-pressure systems coming from the North Atlantic Ocean that create a relatively stable surge over several hours. For each model run (i.e., for each day), the daily maximum water depth at 12 control points distributed along the Mandeo and Mendo rivers (Figure 1) was extracted from the results for a detailed analysis of the inundation levels.

Given the computational cost that running the 2D inundation model every day for several years would imply, a surrogate model based on least squares support vector machines (LS-SVM) regression was developed to reconstruct the time series of daily maximum water depths at the 12 control points. The suitability of the LS-SVM regression technique as a surrogate of the 2D shallow water equations in flood inundation applications was previously evaluated in detail in Bermúdez, Cea, and Puertas (2019). In order to build the LS-SVM surrogate model, we first grouped the time series of the flood drivers in triplets of concurrent river discharge, tidal range and storm surge plus sea level rise. The reason for merging surge and sea level rise is that, as mentioned above, it is the sum of both that is introduced in the hydraulic model. From these series, we selected two representative samples of 250 and 50 characteristic days, which were used respectively to calibrate and validate the LS-SVM regression model (Figure S1 in Supporting Information S1 shows a scatter plot of the samples). Both samples were extracted applying the Maximum Dissimilarity algorithm (Camus et al., 2011; Kennard & Stone, 1969). This clustering algorithm identifies a subset of points comprising the most dissimilar data and, at the same time, distributed fairly evenly across the whole space of variables. It includes, therefore, average and extreme values of the variables. This is important for the calibration of the LS-SVM model, since during the whole time series it will be applied to both average and extreme flow conditions.

Therefore, only a representative sample of 300 characteristic days were simulated with the 2D inundation model and used to calibrate and validate the LS-SVM surrogate model. The use of simulation data instead of field measurements is a common approach when developing surrogate models, due to the need for enough training data to achieve appropriate generalization. However, if enough monitoring data were available, the surrogate model could be trained directly to this data, and the use of a 2D hydraulic model would be avoided. The maximum water depth at each control point obtained with Iber + constituted the dependent variables of the regression models, whereas the predictor variables were derived from the discharge and sea-level time series prescribed at the open boundaries. Based on a previous study in a nearby area (Bermúdez, Cea, & Puertas, 2019), a combination of three parameters was selected to serve as predictors: (a) the maximum daily discharge either in the Mandeo or Mendo rivers, depending on the location of the control point considered; (b) the tidal range; and (c) the sum of the storm surge and the sea-level rise.

The LS-SVM technique has already been used successfully in previous studies (Bermúdez, Cea, & Puertas, 2019; Bermúdez, Cea, & Sopelana, 2019). In this case, the predictions of daily maximum water surface elevation obtained with the LS-SVM model also showed a good agreement with those obtained with the 2D inundation model. The mean and 90th percentile absolute errors were below 10 and 21 cm, respectively, at all points in calibration and validation (Figure S2 in Supporting Information S1). The global mean absolute error (i.e., considering all runs and control points) was 2.5 cm. This demonstrates the suitability of the technique to reconstruct the time series of maximum daily water levels from the time series of the flood drivers.

4. Results and Discussion

4.1. River Discharges

The hydrological model was calibrated and validated with data from the period 2008–2016, as explained in Section 3.6. The results in both the calibration and validation periods were evaluated by means of the following goodness-of-fit coefficients: the Nash-Sutcliffe Efficiency (NSE), the Adapted for high flows Nash-Sutcliffe Efficiency (ANSE), the squared Pearson correlation coefficient (R^2) and the Kling and Gupta Efficiency (KGE). The reader is referred to Gupta et al. (2009); Hoffmann et al. (2004) and Moriasi et al. (2007) for a detailed description of each coefficient.

The simulated hydrographs at an hourly time scale compare well with the observed ones (Figure 4) and are able to capture all the high discharge events, with good estimates of the peak discharge. The NSE and R^2 coefficients are above 0.8, the NSE for high flows is above 0.85, and the KGE is above 0.90 in the validation period. Further details on the model performance are given in Table S1 in Supporting Information S1.

Flow duration curves were computed for the historical and future discharge series (Figure 5 and Figure S5 in Supporting Information S1). All GCMs indicate a future decrease in the medium-low range flows with respect to the historical data. As expected, the magnitude of this decrease is more significant in the RCP 8.5 than in the RCP 4.5 scenario. If we look at the median of the results obtained with the different GCMs (red

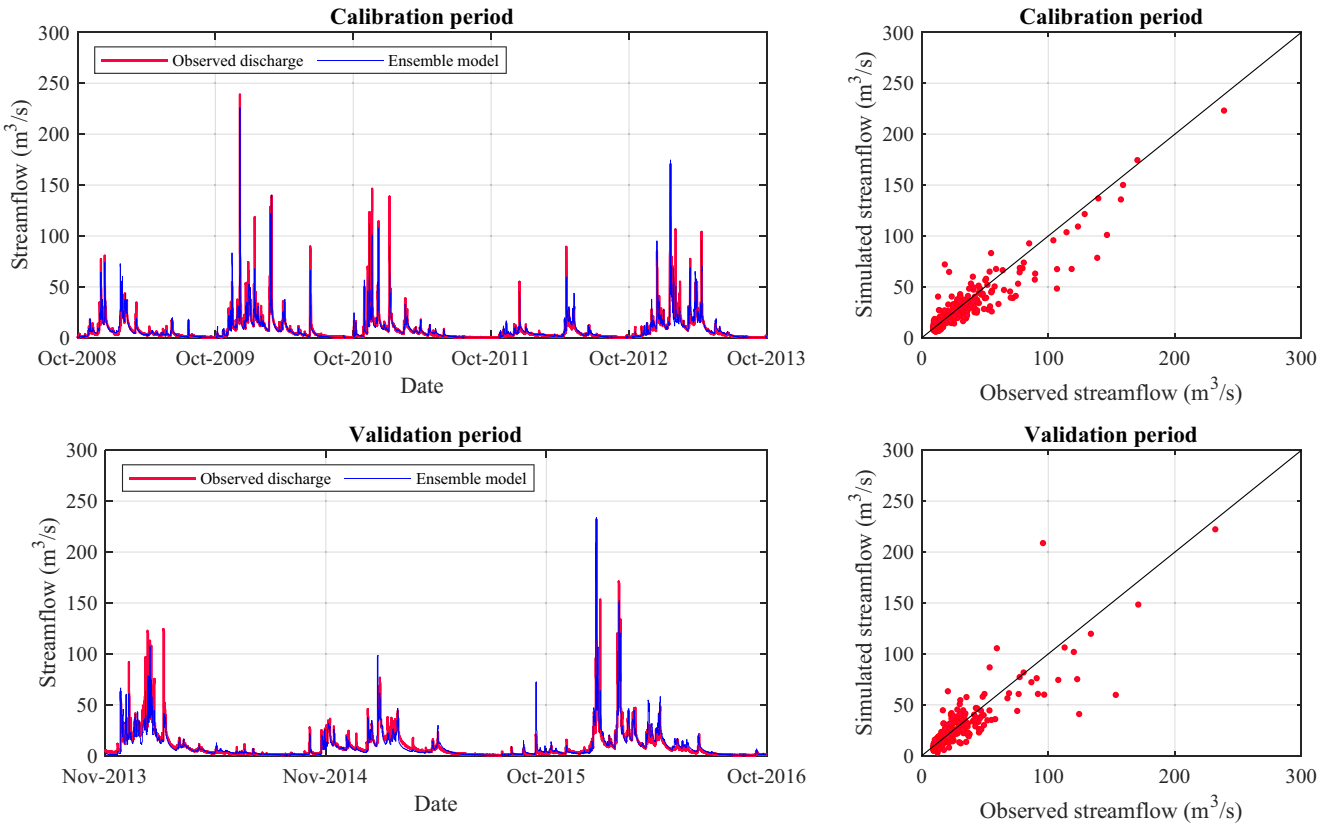

Figure 4. Hydrographs of the calibration and validation of the hydrological model for the Mandeo river (left). Simulated versus observed relative peak flows over threshold corresponding to the 75th percentile (right).

lines in Figure 5), we find that the discharge of 1 m^3/s is exceeded 70% of the time in the RCP 8.5 scenario and around 77% of the time in RCP 4.5. The same discharge is exceeded 85% of the time in the historical period. If we look at even lower discharges, as those that are exceeded 90% of the time, we find values of 0.8, 0.5, and 0.3 m^3/s for the historical, RCP 4.5 and RCP 8.5 scenarios, respectively.

Since low flows in this basin occur in the summer, these results point to a decrease in future flows in this season. On the contrary, maximum discharges in the winter season tend to increase in the future scenarios, as can be deduced from the flow duration curves. For example, the discharge exceeded 1% of the time in the historical series is 62 m^3/s, while in the future period, according to the median of all the GCMs results, this discharge is exceeded 1.6% and 1.8% of the time in RCP 4.5 and RCP 8.5, respectively.

In order to analyze the extreme values of discharge, the annual maxima extracted from the time series were used to derive extreme value estimates by fitting a Gumbel distribution to the historical data and to the future scenarios (Figure 6). In the case of the RCP 4.5 and RCP 8.5 future scenarios, the annual maxima were extracted for each GCMs projection, and then the Gumbel distributions were fit to the 10th, 50th, and 90th percentiles of the point estimates for each return period. The projections obtained with the majority of GCMs agree in predicting an increase in extreme river discharges for all return periods up to 30 years, but the magnitude of this increase varies widely between GCMs, and thus so does the difference between the 10th and 90th percentile estimates. Changes are in general stronger for the RCP 8.5 scenario, with median projections showing roughly a ratio of 1.5 with respect to the historical scenario (i.e., a 50% increase in the discharge for a 25-year return period). Figure 6 can be used to evaluate the future increase in the frequency of occurrence of high discharges. For instance, according to the historical data, in the Mandeo basin the discharge of 400 m^3/s will occur on average once every 26 years. However, in the future period the same discharge will occur, on average, once every 9 years according to the RCP 4.5 median estimate. If we look at the RCP 8.5 median estimate, the 400 m^3/s discharge will occur every 6 years. Similar trends are obtained in

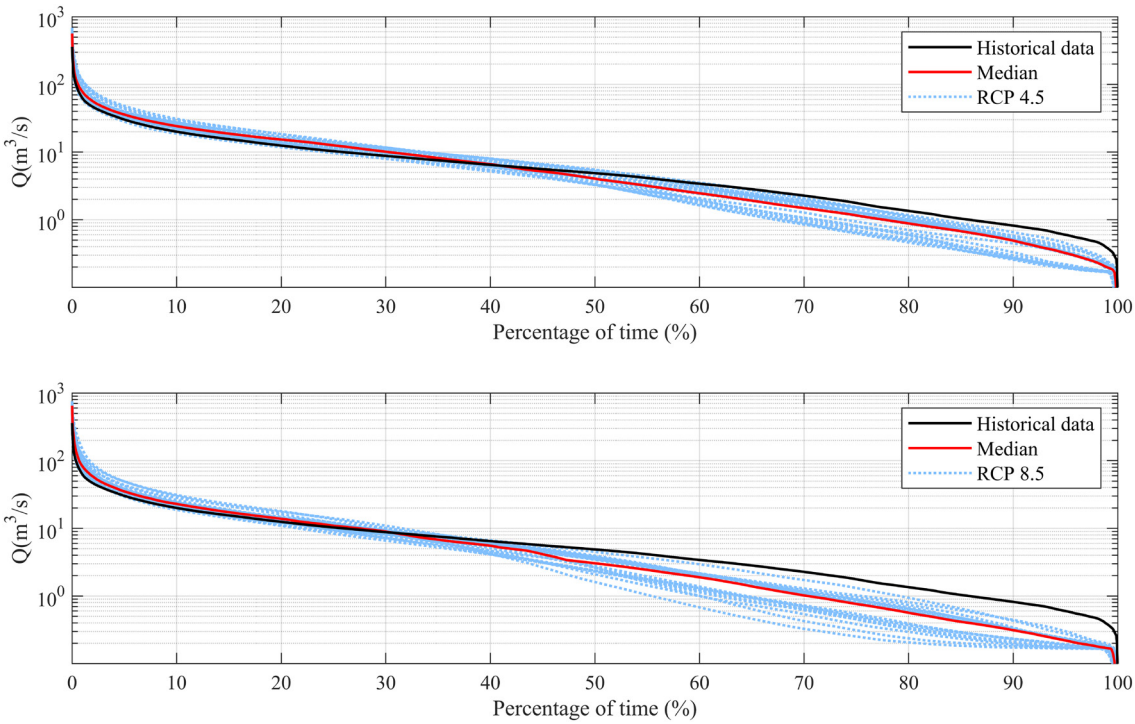

Figure 5. Flow duration curve for the Mandeo river in the historical and future scenarios: RCP4.5 (up) and RCP8.5 (down).

the smaller Mendo catchment (Figure 6), although the relative increase in the magnitude and frequency of high discharges is not as high as in the Mandeo.

So, despite the uncertainties in the projections obtained with the different GCMs for the two RCP scenarios, these results clearly point toward an increase in the frequency and magnitude of high flows in both basins.

4.2. Sea Levels

Extreme sea levels in the area are driven by the astronomical tide and storm surge. In this study, the same tidal range series were applied for both the historical and future scenarios, which are based on present-day tidal harmonic constituents. Although the propagation of tides in certain estuaries and rivers can be affected by changes in water depth due to SLR (Schindelegger et al., 2018), the change is expected to be minor in the estuaries of this region, according to the trend in the tidal amplitude of −0.6 mm/yr observed between 2000 and 2015 (Serrano et al., 2020) and the results of modeling studies (Pickering et al., 2017).

On the other hand, future storm surges were calculated by downscaling GCM projections of SLP, and can therefore differ from present conditions. A statistical analysis of the entire reconstructed storm surge series was performed, and extreme values were calculated (Figure 7). Similarly to the analysis of river discharges, a Gumbel distribution was fitted to the annual maxima of the historical and future scenarios, and 10th, 50th, and 90th percentiles of all the GCMs projections were calculated for each return period in the RCP 4.5 and RCP 8.5 scenarios. The results suggest that the extreme storm surge heights will remain stable or decrease slightly, which is consistent with previous studies in the Atlantic coast of Europe (Vousdoukas et al., 2016). In most GCM projections, the differences with respect to the historical return period value are less than 10 cm. Minor differences are also found between RCP4.5 and 8.5 scenarios.

Despite the minor changes in tide and storm surge, extreme sea levels will also change due to the expected SLR in the upcoming years. According to the projections used in this study (Section 3.2), the mean sea level at this location is predicted to rise 0.50 m in RCP4.5 and 0.69 m in RCP8.5 by 2100. Based on the above, the SLR constitutes the main driver of future changes in sea-level at the study site. It should also be noted that we are considering the ensemble mean of the SLR projections for the two RCP scenarios. The consideration

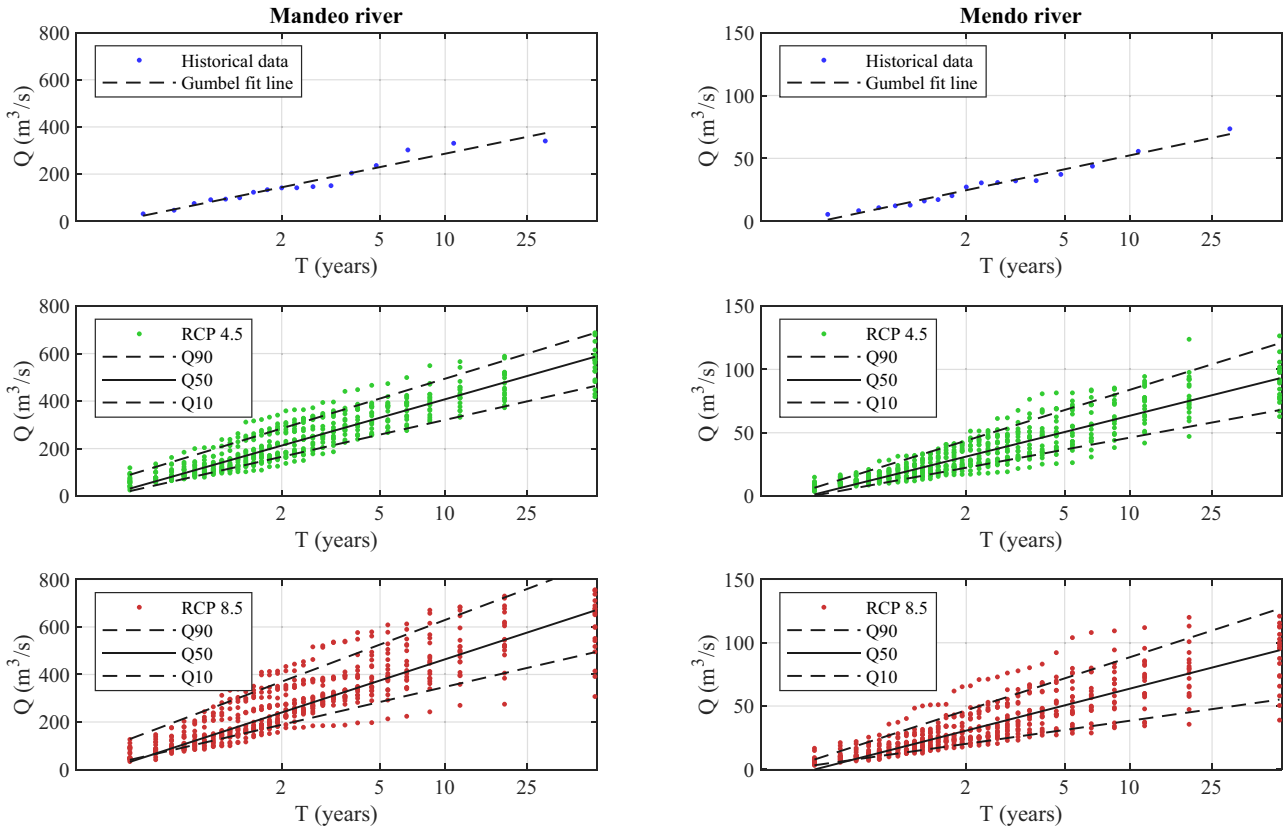

Figure 6. Annual peak discharge frequency curves for the historical data (2001–2017) and future projections (2071–2100) according to scenarios RCP 4.5 and RCP 8.5, in the Mandeo (left) and Mendo (right) rivers. Dashed lines Q90, Q50, and Q10 are the 10th, 50th, and 90th percentiles of the point estimates for each return period.

of the upper limit of the confidence intervals (see Figure S4 in Supporting Information S1), or even more extreme scenarios outside that likely range (Church et al., 2013), would enhance the dominant role of the SLR in the future frequency of extreme sea levels.

4.3. Water Depth

The trend of future change in flood levels at this site can be inferred from the changes in sea level and discharge presented in Sections 4.1 and 4.2. However, these drivers need to be jointly simulated with a flood inundation model in order to quantify the changes in water depths. The methodology described in Section 3.7, which combines a 2D inundation model with a LS-SVM model, was followed in this study for this purpose.

The simulated water surface elevation (WSE) values were plotted as a function of the following flood drivers: the river discharge (Figure 8a), the sum of the storm surge and sea-level rise (Figure 8b), and the tidal range (Figure S6 in Supporting Information S1). The water level at the control points located downstream the confluence of Mandeo and Mendo is driven by storm surge and tides (Figure 8b and Figure S6 in Supporting Information S1), as well as the sea-level rise in the case of the future scenarios. Thus, at those control points, high water levels can occur under any discharge condition (Figure 8a) associated with high sea levels. On the contrary, further upstream, high water levels are always associated with high discharges. The role played by the river discharge significantly increases as we move upstream along the river reach (from P4 to P8 on the river Mandeo, and from P11 to P9 in river Mendo), as shown by the steeper slopes of the scatter plots. Although this behavior can be seen in the historical records, it is more evident in future estimates due to the significant increase in the projected discharges. In this upper part of the reach, high water levels can occur even during low tidal range conditions and low surges, driven only by very high river flows, as reflected in the large spread in the high water level region of the S + SLR scatter plots (Figure 8b).

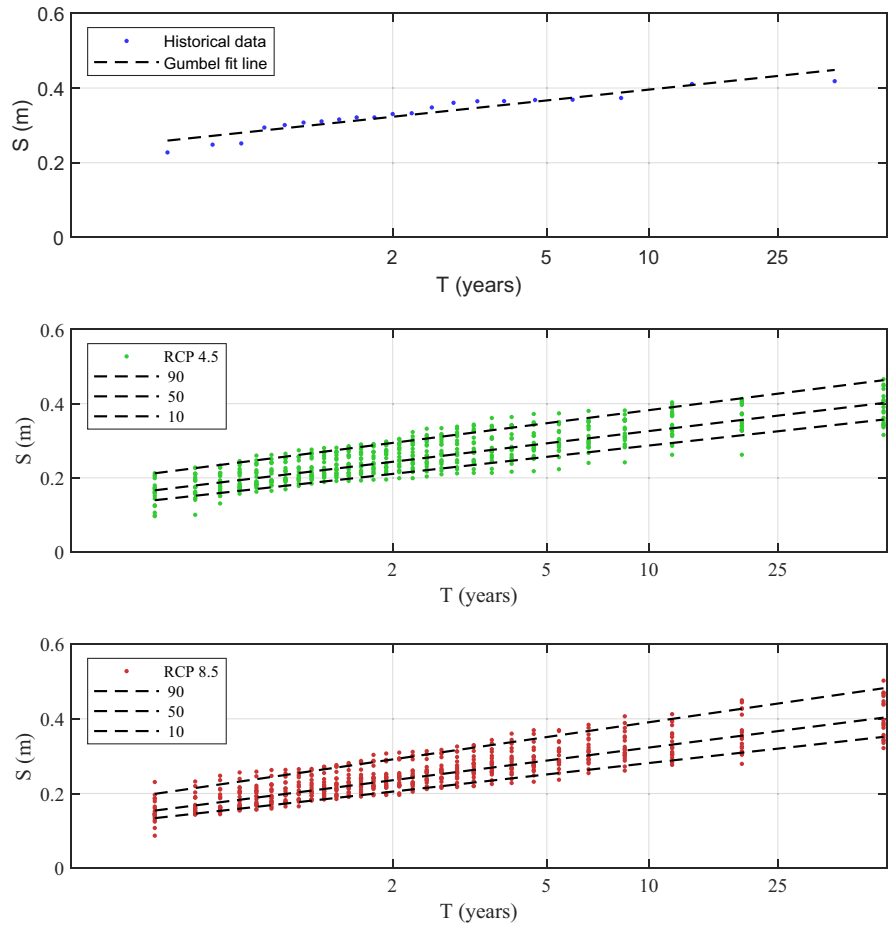

Figure 7. Annual storm surge frequency curves for the historical data (2001–2017) and future projections (2071–2100) according to scenarios RCP 4.5 and RCP 8.5. Dashed lines 90, 50, and 10 are the 10th, 50th, and 90th percentiles of the point estimates for each return period.

The behavior observed in the upstream points of both rivers (Mandeo and Mendo) is very similar. However, in the river Mendo, a stronger relationship with little scatter is evident between Q and WSE for the upper range of discharges (approximately for Qs larger than 50 m^3/s). The flow rate exerts almost total control over the WSE values in this range. This can be explained by the steeper bed slope of this river reach, with bottom levels located at a higher elevation, which is less affected by backwater effects due to high sea levels. The behavior is otherwise very similar to that of the river Mandeo, so that in the following analyses, in the interests of clarity, only the results of the river Mandeo are presented.

The potential future changes in the normal and extreme WSE values at the different control points were analyzed. A statistical analysis of the entire reconstructed WSE series was performed, and the median and the 99.7th percentiles were compared as relevant estimators (Table 3). The results show similar future increases in the median water levels for all points, which are in the order of 0.4 m for RCP4.5 and 0.5 m for RCP8.5 scenarios. These increases reflect the projected rise in the mean sea level and the backwater propagation at the reach. As explained in Section 4.2, we consider the ensemble mean of the SLR projections for the two scenarios. The consideration of upper SLR projections would result in significantly higher increases in the median water levels. On the contrary, there are significant differences between points in the 99.7th percentile values obtained from the reconstructed WSE series. The upstream points (P5 to P8) present greater water level increases than locations further downstream, since they are more affected by the projected increases in river discharges (Figure 8a).

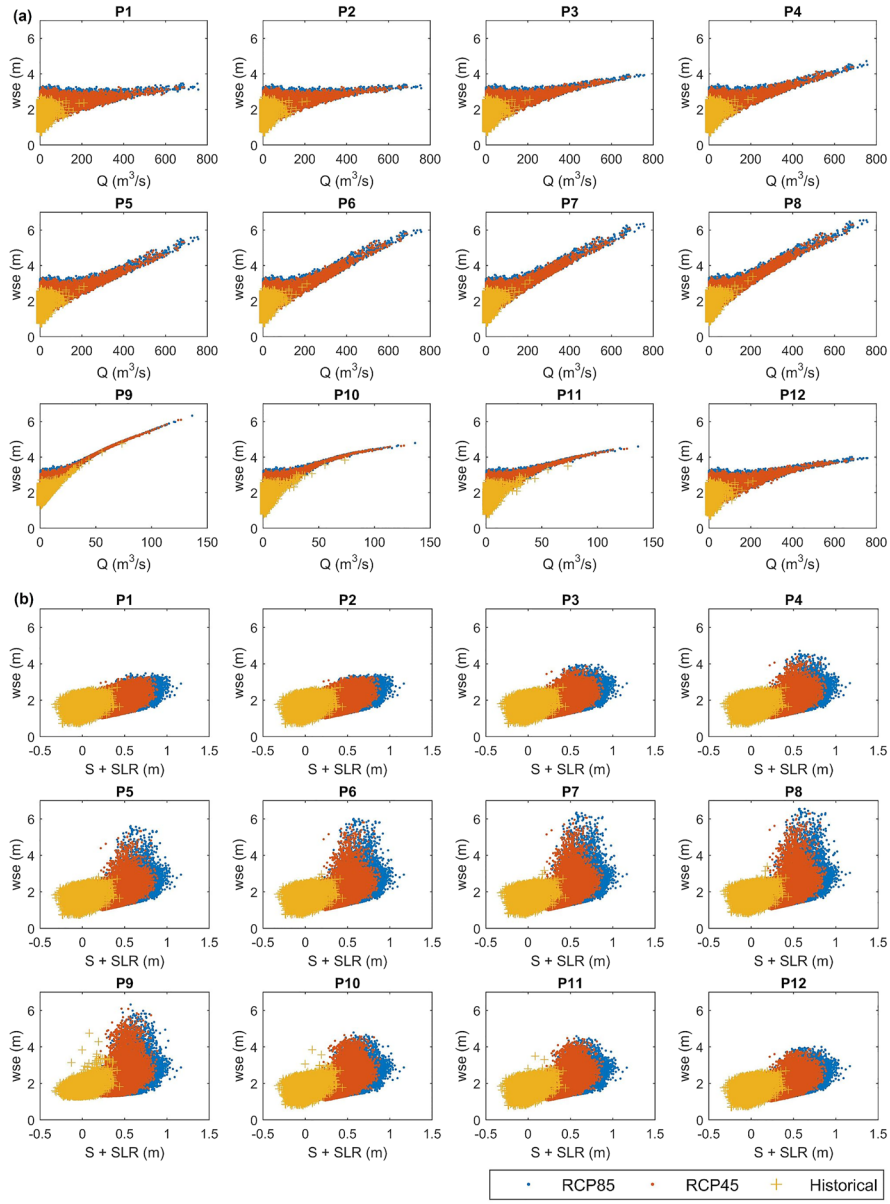

Figure 8. Daily maximum water surface elevation at the different control points versus: (a) discharge and (b) sum of the storm surge and sea-level rise, for historical and RCP4.5 and RCP8.5 scenarios. Note: the discharge plotted is the one used as predictor in the LS-SVM model, which corresponds to the Mandeo river for points P1-P8 and P12, and the river Mendo for points P9-P11.

In a subsequent step, the annual maxima at each control point were extracted from the reconstructed wse time series. They were used to obtain the mean annual maximum water level (MAM) (Figure 9) and to derive extreme value estimates for return periods up to 30 years (Figure 10).

MAMs at all points are predicted to increase in the future (Figure 9). At points close to the sea (P1 to P3), the MAM projections are relatively similar between RCPs. The SLR drives the increases in MAMs with respect to the historical scenario, and the differences in MAMs between RCPs respond to the differences in SLR magnitude between the scenarios. MAM projections exhibit very little spread between GCM runs in each scenario due to the minor differences in storm surge projections between runs, as shown in Section 4.2. Further inland (points P4 to P8), extreme water levels are dominated by the discharge, which is predicted to increase significantly, and the differences in MAMs with respect to the historical scenarios are larger. As

Table 3
Median and 99.7th Percentile of the WSE Time Series at Each Control Point

	WSE (m)	P1	P2	P3	P4	P5	P6	P7	P8
Median	Historical	1.71	1.71	1.71	1.72	1.73	1.75	1.77	1.84
	RCP4.5	2.09	2.10	2.10	2.10	2.11	2.11	2.13	2.19
	RCP8.5	2.22	2.23	2.23	2.23	2.24	2.25	2.26	2.32
	Difference RCP4.5—historical	0.39	0.39	0.39	0.39	0.38	0.37	0.36	0.36
	Difference RCP8.5—historical	0.52	0.52	0.52	0.52	0.52	0.50	0.49	0.49
P99.7	Historical	2.50	2.50	2.52	2.53	2.54	2.56	2.56	2.63
	RCP4.5	2.92	2.94	2.96	2.98	3.04	3.14	3.21	3.39
	RCP8.5	3.08	3.09	3.12	3.14	3.24	3.38	3.52	3.73
	Difference RCP4.5—historical	0.42	0.43	0.44	0.45	0.50	0.58	0.64	0.76
	Difference RCP8.5—historical	0.58	0.59	0.59	0.61	0.70	0.82	0.96	1.10

Note. In the RCP scenarios, where a set of 19 GCMs is considered, the values correspond to the median 99.7th percentile of all GCMs. GCM, Global climate model; WSE, Water surface elevation.

shown in Section 4.1, discharge projections also display a large spread between models. As a consequence, there is a higher variability in the MAM projections at these upstream points.

Similar observations can be made on the flood frequency analysis (Figure 10). The direction of future change in extreme value estimates is consistent between GCMs, showing a general increase in water levels, especially for the RCP8.5. At the inland points, the magnitude of change varies widely between GCMs, since they strongly influence the river discharge projections.

5. Conclusions

High water levels in coastal river areas originate from complex interactions between coastal and inland drivers. In the context of changing climate, reliable methods capable of dealing with this complexity are urgently needed to assess future flood conditions in these already flood-prone areas. The method proposed in this study involves an assessment of historical and future flooding conditions in coastal river areas by using a continuous simulation approach that considers seasonality and the correlation between flood drivers. It can be used to evaluate potential future changes in flood hazard and to identify the drivers that are

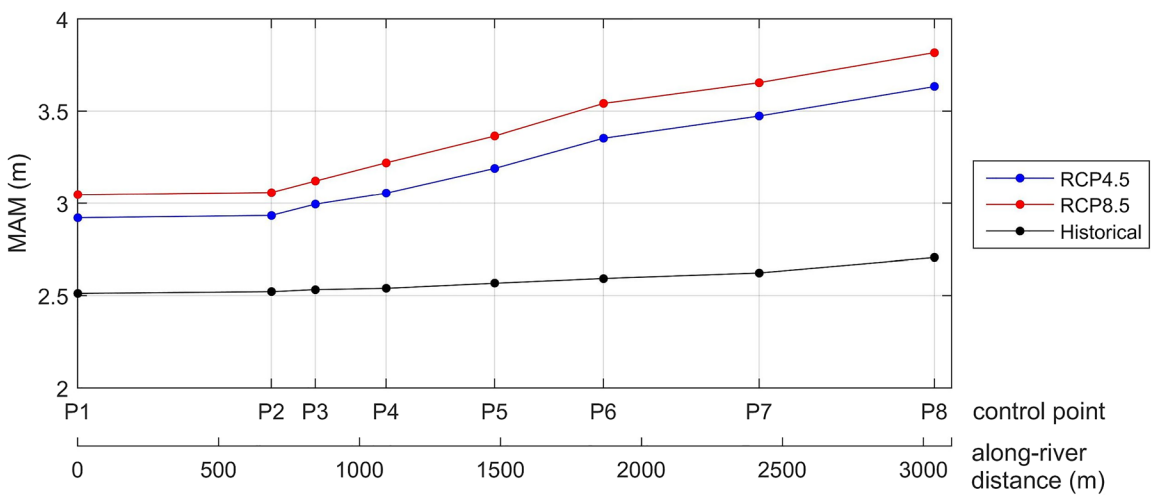

Figure 9. Longitudinal profile of mean annual maxima water levels obtained for the historical and future scenarios. For the future scenarios, the median percentiles considering all global climate models are plotted.

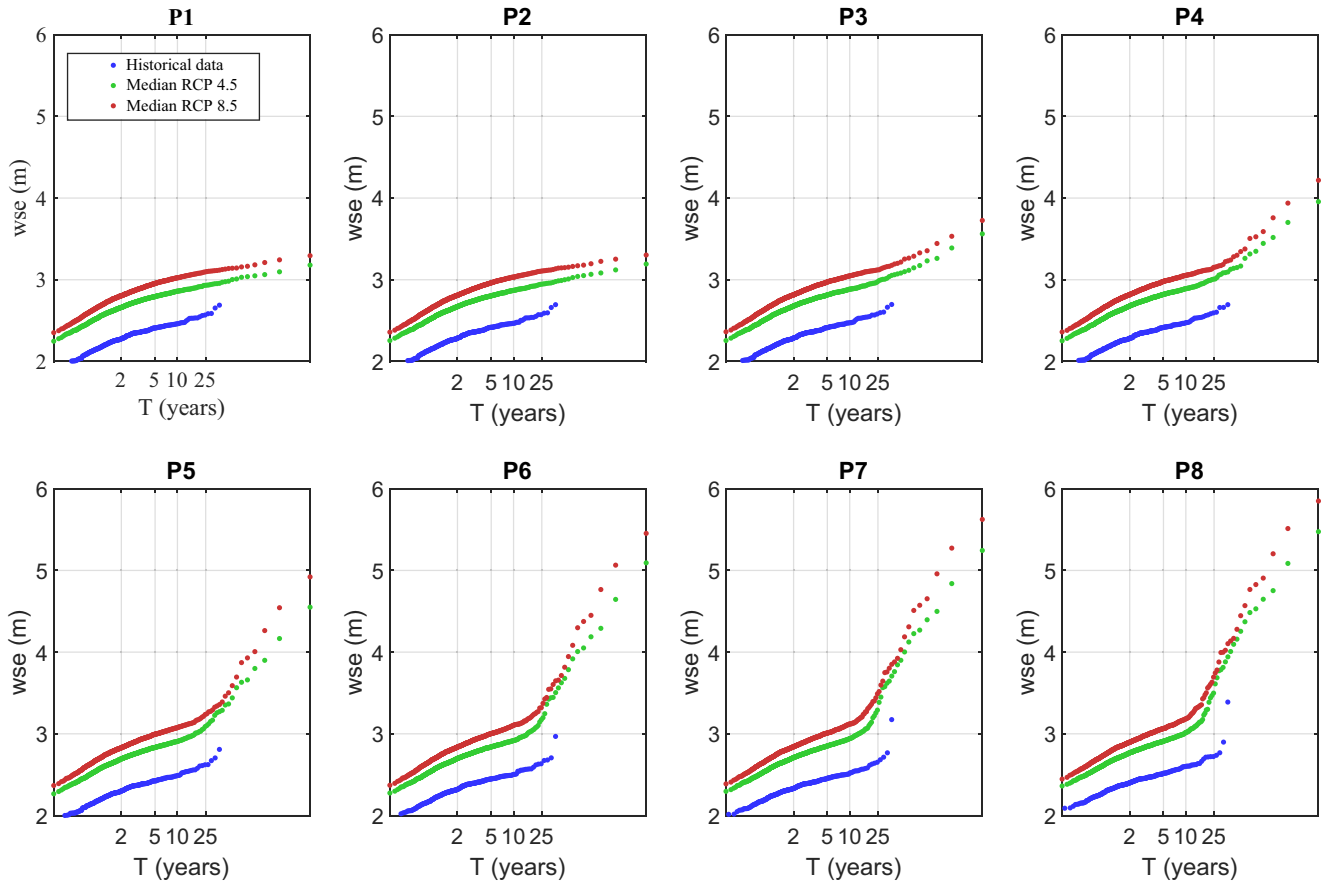

Figure 10. Flood frequency analysis for the annual maximum water level in the historical and future scenarios. Only the median return period values considering all global climate models are plotted for the RCP4.5 and RCP8.5 scenarios.

largely responsible for these changes. The results can ultimately inform adaptation planning in regions with compound flooding potential.

The proposed methodology was applied to a coastal river reach in NW Spain, located at the confluence of the rivers Mandeo and Mendo, and which suffers from compound flooding due to high river discharges and sea levels. The main conclusions that can be drawn from the results obtained in this case study can be summarized as follows:

1. High water levels downstream the confluence of Mandeo and Mendo rivers are driven by sea levels, whereas river discharge is dominant in the upstream part of the reach. The methodology can be used to evaluate the relative impact of sea level and river discharge over the river reach under study.
2. Local future projections show a small decrease in storm surge extremes with respect to the historical period. A larger change toward increasing discharge extremes is predicted, although the magnitude of change is highly GCM dependent.
3. The SLR drives the future increases in extreme water levels in the outer part of the study area. On the contrary, river discharge drives the water level increase in the inner part of the study area. The variability in the discharge projections results in a large impact range on the water surface elevation.
4. It is generally expected that the increases in extreme water levels in coastal areas will be mostly a result of the SLR. However, climate change affects other flood drivers which can play a relevant role in water depth extremes in regions with compound flooding potential, as evidenced in this case by the river discharge.

We do, nevertheless, acknowledge the uncertainty in the future projections from GCMs that the method relies on, and thus the need to re-assess the results obtained as improved projections become available.

Data Availability Statement

Data for this research are indicated in Table 1 and are available through the sources listed therein.

Acknowledgments
M. Bermúdez acknowledges funding from EU's Horizon 2020 Programme under Marie Skłodowska-Curie Grant Agreement 754446 and UGR Research and Knowledge Transfer Fund—Athenea3i. Funding for open access charge: Universidad de Granada/CBUA.

References

Andraos, C., & Najem, W. (2020). Multi-model approach for reducing uncertainties in rainfall-runoff models BT. In P. Gourbesville, & G. Caignaert, (Eds.), *Advances in hydroinformatics* (pp. 545–557). Singapore: Springer Singapore.

Areu-Rangel, O., Cea, L., Bonasia, R., & Espinosa-Echavarria, V. (2019). Impact of urban growth and changes in land use on river flood hazard in Villahermosa, Tabasco (Mexico). *Water*, *11*(2), 304. https://doi.org/10.3390/w11020304

Bermúdez, M., Cea, L., & Puertas, J. (2019). A rapid flood inundation model for hazard mapping based on least squares support vector machine regression. *Journal of Flood Risk Management*, *12*, e12522. https://doi.org/10.1111/jfr3.12522

Bermúdez, M., Cea, L., & Sopelana, J. (2019). Quantifying the role of individual flood drivers and their correlations in flooding of coastal river reaches. *Stochastic Environmental Research and Risk Assessment*, *33*(10), 1851–1861. https://doi.org/10.1007/s00477-019-01733-8

Bermúdez, M., Cea, L., Van Uytven, E., Willems, P., Farfán, J. F., & Puertas, J. (2020). A robust method to update local river inundation maps using global climate model output and weather typing based statistical downscaling. *Water Resources Management*, *34*, 1–18. https://doi.org/10.1007/s11269-020-02673-7

Bermúdez, M., Neal, J. C., Bates, P. D., Coxon, G., Freer, J. E., Cea, L., & Puertas, J. (2017). Quantifying local rainfall dynamics and uncertain boundary conditions into a nested regional-local flood modeling system. *Water Resources Research*, *53*(4), 2770–2785. https://doi.org/10.1002/2016WR019903

Bevacqua, E., Maraun, D., Hobæk Haff, I., Widmann, M., & Vrac, M. (2017). Multivariate statistical modelling of compound events via pair-copula constructions: Analysis of floods in Ravenna (Italy). *Hydrology and Earth System Sciences*, *21*(6), 2701–2723. https://doi.org/10.5194/hess-21-2701-2017

Bevacqua, E., Maraun, D., Vousdoukas, M. I., Voukouvalas, E., Vrac, M., Mentaschi, L., & Widmann, M. (2019). Higher probability of compound flooding from precipitation and storm surge in Europe under anthropogenic climate change. *Science Advances*, *5*(9). https://doi.org/10.1126/sciadv.aaw5531

Bevacqua, E., Vousdoukas, M. I., Shepherd, T. G., & Vrac, M. (2020). Brief communication: The role of using precipitation or river discharge data when assessing global coastal compound flooding. *Natural Hazards and Earth System Sciences*, *20*(6), 1765–1782. https://doi.org/10.5194/nhess-20-1765-2020

Bladé, E., Cea, L., Corestein, G., Escolano, E., Puertas, J., Vázquez-Cendón, E., et al. (2014). Iber: Herramienta de simulación numérica del flujo en ríos. *Revista Internacional de Métodos Numéricos Para Cálculo y Diseño En Ingeniería*, *30*(1), 1–10. https://doi.org/10.1016/j.rimni.2012.07.004

Brocca, L., Liersch, S., Melone, F., Moramarco, T., & Volk, M. (2013). Application of a model-based rainfall-runoff database as efficient tool for flood risk management. *Hydrology and Earth System Sciences*, *17*(8), 3159–3169. https://doi.org/10.5194/hess-17-3159-2013

Camici, S., Tarpanelli, A., Brocca, L., Melone, F., & Moramarco, T. (2011). Design soil moisture estimation by comparing continuous and storm-based rainfall-runoff modeling. *Water Resources Research*, *47*(5). https://doi.org/10.1029/2010WR009298

Camus, P., Mendez, F. J., Medina, R., & Cofiño, A. S. (2011). Analysis of clustering and selection algorithms for the study of multivariate wave climate. *Coastal Engineering*, *58*(6), 453–462. https://doi.org/10.1016/j.coastaleng.2011.02.003

Cea, L., & Fraga, I. (2018). Incorporating antecedent moisture conditions and intraevent variability of rainfall on flood frequency analysis in poorly gauged basins. *Water Resources Research*, *54*(11), 8774–8791. https://doi.org/10.1029/2018WR023194

Cea, L., & French, J. R. (2012). Bathymetric error estimation for the calibration and validation of estuarine hydrodynamic models. *Estuarine, Coastal and Shelf Science*, *100*, 124–132. https://doi.org/10.1016/J.ECSS.2012.01.004

Church, J. A., Clark, P. U., Cazenave, A., Gregory, J. M., Jevrejeva, S., Levermann, A., et al. (2013). *Sea-level rise by 2100*. American Association for the Advancement of Science. https://doi.org/10.1126/science.342.6165.1445-a

Couasnon, A., Eilander, D., Muis, S., Veldkamp, T. I. E., Haigh, I. D., Wahl, T., et al. (2020). Measuring compound flood potential from river discharge and storm surge extremes at the global scale. *Natural Hazards and Earth System Sciences*, *20*(2), 489–504. https://doi.org/10.5194/nhess-20-489-2020

CRED, & UNISDR. (2015). *The human cost of weather related disasters 1995–2015*. https://doi.org/10.13140/RG.2.2.17677.33769

Davies, J. L. (1964). A morphogenic approach to world shorelines. *Zeitschrift Fur Geomorphologie*, *8*, 127–142. https://doi.org/10.1127/zfg/mortensen/8/1964/127

Devlin, A. T., Jay, D. A., Talke, S. A., Zaron, E. D., Pan, J., & Lin, H. (2017). Coupling of sea level and tidal range changes, with implications for future water levels. *Scientific Reports*, *7*(1), 17021. https://doi.org/10.1038/s41598-017-17056-z

Ekström, M., Grose, M. R., & Whetton, P. H. (2015). An appraisal of downscaling methods used in climate change research. *Wiley Interdisciplinary Reviews: Climate Change*, *6*(3), 301–319. https://doi.org/10.1002/wcc.339

Ensign, S. H., & Noe, G. B. (2018). Tidal extension and sea-level rise: Recommendations for a research agenda. *Frontiers in Ecology and the Environment*, *16*(1), 37–43. https://doi.org/10.1002/fee.1745

Farfán, J. F., Palacios, K., Ulloa, J., & Avilés, A. (2020). A hybrid neural network-based technique to improve the flow forecasting of physical and data-driven models: Methodology and case studies in Andean watersheds. *Journal of Hydrology: Regional Studies*, *27*, 1–18. https://doi.org/10.1016/j.ejrh.2019.100652

Fowler, H. J., Blenkinsop, S., & Tebaldi, C. (2007). Linking climate change modelling to impacts studies: Recent advances in downscaling techniques for hydrological modelling. *International Journal of Climatology*, *27*(12), 1547–1578. https://doi.org/10.1002/joc.1556

Ganguli, P., & Merz, B. (2019). Extreme coastal water levels exacerbate fluvial flood hazards in northwestern Europe. *Scientific Reports*, *9*(1), 1–14. https://doi.org/10.1038/s41598-019-49822-6

García-Feal, O., González-Cao, J., Gómez-Gesteira, M., Cea, L., Domínguez, J., Formella, A., & Formella, A. (2018). An accelerated tool for flood modelling based on Iber. *Water*, *10*(10), 1459. https://doi.org/10.3390/w10101459

Gourley, J. J., & Vieux, B. E. (2006). A method for identifying sources of model uncertainty in rainfall-runoff simulations. *Journal of Hydrology*, *327*(1–2), 68–80. https://doi.org/10.1016/j.jhydrol.2005.11.036

Gupta, H. V., Kling, H., Yilmaz, K. K., & Martinez, G. F. (2009). Decomposition of the mean squared error and NSE performance criteria: Implications for improving hydrological modelling. *Journal of Hydrology*, *377*(1–2), 80–91. https://doi.org/10.1016/j.jhydrol.2009.08.003

Hendry, A., Haigh, I. D., Nicholls, R. J., Winter, H., Neal, R., Wahl, T., et al. (2019). Assessing the characteristics and drivers of compound flooding events around the UK coast. *Hydrology and Earth System Sciences*, *23*(7), 3117–3139. https://doi.org/10.5194/hess-23-3117-2019

Hoffmann, L., El Idrissi, A., Pfister, L., Hingray, B., Guex, F., Musy, A., et al. (2004). Development of regionalized hydrological models in an area with short hydrological observation series. *River Research and Applications*, *20*(3), 243–254. https://doi.org/10.1002/rra.774
Jenkinson, A. F., & Collison, F. (1977). *An initial climatology of gales over the North Sea*.
Kennard, R. W., & Stone, L. A. (1969). Computer aided design of experiments. *Technometrics*, *11*(1), 137–148. https://doi.org/10.2307/1266770
Koks, E. E., Jongman, B., Husby, T. G., & Botzen, W. J. W. (2015). Combining hazard, exposure and social vulnerability to provide lessons for flood risk management. *Environmental Science and Policy*, *47*, 42–52. https://doi.org/10.1016/j.envsci.2014.10.013
Kumar, A., Singh, R., Jena, P. P., Chatterjee, C., & Mishra, A. (2015). Identification of the best multi-model combination for simulating river discharge. *Journal of Hydrology*, *525*, 313–325. https://doi.org/10.1016/j.jhydrol.2015.03.060
Li, W., & Sankarasubramanian, A. (2012). Reducing hydrologic model uncertainty in monthly streamflow predictions using multimodel combination. *Water Resources Research*, *48*(12), 1–17. https://doi.org/10.1029/2011WR011380
Li, Z., Yu, J., Xu, X., Sun, W., Pang, B., & Yue, J. (2018). Multi-model ensemble hydrological simulation using a BP Neural Network for the upper Yalongjiang River Basin, China. *Proceedings of the International Association of Hydrological Sciences*, *379*, 335–341. https://doi.org/10.5194/piahs-379-335-2018
Maraun, D., Wetterhall, F., Ireson, A. M., Chandler, R. E., Kendon, E. J., Widmann, M., et al. (2010). Precipitation downscaling under climate change: Recent developments to bridge the gap between dynamical models and the end user. *Reviews of Geophysics*, *48*(3). https://doi.org/10.1029/2009RG000314
Menéndez, M., & Woodworth, P. L. (2010). Changes in extreme high water levels based on a quasi-global tide-gauge data set. *Journal of Geophysical Research*, *115*(C10), C10011. https://doi.org/10.1029/2009JC005997
Moriasi, D. N., Arnold, J. G., Van Liew, M. W., Binger, R. L., Harmel, R. D., & Veith, T. L. (2007). Model evaluation guidelines for systematic quantification of accuracy in watershed simulations. *Transactions of the ASABE*, *50*(3), 885–900. https://doi.org/10.13031/2013.23153
Paprotny, D., Vousdoukas, M. I., Morales-Nápoles, O., Jonkman, S. N., & Feyen, L. (2020). Pan-European hydrodynamic models and their ability to identify compound floods. *Natural Hazards*, *101*(3), 933–957. https://doi.org/10.1007/s11069-020-03902-3
Pérez Gómez, B., & Begoña. (2014). *Design and implementation of an operational sea level monitoring and forecasting system for the Spanish coast*. University of Cantabria. Retrieved From https://repositorio.unican.es/xmlui/handle/10902/5876
Pickering, M. D., Horsburgh, K. J., Blundell, J. R., Hirschi, J. J. M., Nicholls, R. J., Verlaan, M., & Wells, N. C. (2017). The impact of future sea-level rise on the global tides. *Continental Shelf Research*, *142*, 50–68. https://doi.org/10.1016/J.CSR.2017.02.004
Pierce, D. W., Barnett, T. P., Santer, B. D., & Gleckler, P. J. (2009). Selecting global climate models for regional climate change studies. *Proceedings of the National Academy of Sciences*, *106*(21), 8441–8446. https://doi.org/10.1073/PNAS.0900094106
Rueda, A., Vitousek, S., Camus, P., Tomás, A., Espejo, A., Losada, I. J., et al. (2017). A global classification of coastal flood hazard climates associated with large-scale oceanographic forcing. *Scientific Reports*, *7*(1), 5038. https://doi.org/10.1038/s41598-017-05090-w
Schindelegger, M., Green, J. A. M., Wilmes, S.-B., & Haigh, I. D. (2018). Can we model the effect of observed sea level rise on tides? *Journal of Geophysical Research: Oceans*, *123*(7), 4593–4609. https://doi.org/10.1029/2018JC013959
Seneviratne, S. I., Nicholls, N., Easterling, D., Goodess, C. M., Kanae, S., Kossin, J., et al. (2012). Changes in climate extremes and their impacts on the natural physical environment. In C. B. Field, et al. (Eds), *Managing the risks of extreme events and disasters to advance climate change adaptation. A special report of working groups I and II of the intergovernmental panel on climate change (IPCC)*. (pp. 23–109). Cambridge, UK, and New York, NY: Cambridge University Press.
Serrano, M. A., Cobos, M., Magaña, P. J., & Díez-Minguito, M. (2020). Sensitivity of Iberian estuaries to changes in sea water temperature, salinity, river flow, mean sea level, and tidal amplitudes. *Estuarine, Coastal and Shelf Science*, *236*, 106624. https://doi.org/10.1016/j.ecss.2020.106624
Sillmann, J., Kharin, V. V., Zhang, X., Zwiers, F. W., & Bronaugh, D. (2013). Climate extremes indices in the CMIP5 multimodel ensemble: Part 1. Model evaluation in the present climate. *Journal of Geophysical Research: Atmospheres*, *118*(4), 1716–1733. https://doi.org/10.1002/JGRD.50203
Sopelana, J., Cea, L., & Ruano, S. (2018). A continuous simulation approach for the estimation of extreme flood inundation in coastal river reaches affected by meso- and macrotides. *Natural Hazards*, *93*(3), 1337–1358. https://doi.org/10.1007/s11069-018-3360-6
Sweet, W. V., & Park, J. (2014). From the extreme to the mean: Acceleration and tipping points of coastal inundation from sea level rise. *Earth's Future*, *2*(12), 579–600. https://doi.org/10.1002/2014ef000272
Tabari, H. (2020). Climate change impact on flood and extreme precipitation increases with water availability. *Scientific Reports*, *10*(1), 1–10. https://doi.org/10.1038/s41598-020-70816-2
Tebaldi, C., Strauss, B. H., & Zervas, C. E. (2012). Modelling sea level rise impacts on storm surges along US coasts. *Environmental Research Letters*, *7*(1), 014032. https://doi.org/10.1088/1748-9326/7/1/014032
Valle-Levinson, A., Olabarrieta, M., & Heilman, L. (2020). Compound flooding in Houston-Galveston Bay during Hurricane Harvey. *Science of the Total Environment*, *747*, 141272. https://doi.org/10.1016/j.scitotenv.2020.141272
vanden Hurk, B., Hewitt, C., Jacob, D., Bessembinder, J., Doblas-Reyes, F., & Döscher, R. (2018). The match between climate services demands and Earth System Models supplies. *Climate Services*, *12*, 59–63. https://doi.org/10.1016/J.CLISER.2018.11.002
Viney, N. R., Bormann, H., Breuer, L., Bronstert, A., Croke, B. F. W., Frede, H., et al. (2009). Assessing the impact of land use change on hydrology by ensemble modelling (LUCHEM) II: Ensemble combinations and predictions. *Advances in Water Resources*, *32*(2), 147–158. https://doi.org/10.1016/j.advwatres.2008.05.006
Vousdoukas, M. I., Mentaschi, L., Voukouvalas, E., Verlaan, M., & Feyen, L. (2017). Extreme sea levels on the rise along Europe's coasts. *Earth's Future*, *5*, 304–323. https://doi.org/10.1002/2016EF000505
Vousdoukas, M. I., Voukouvalas, E., Annunziato, A., Giardino, A., & Feyen, L. (2016). Projections of extreme storm surge levels along Europe. *Climate Dynamics*, *47*(9–10), 3171–3190. https://doi.org/10.1007/s00382-016-3019-5
Ward, P. J., Couasnon, A., Eilander, D., Haigh, I. D., Hendry, A., Muis, S., et al. (2018). Dependence between high sea-level and high river discharge increases flood hazard in global deltas and estuaries. *Environmental Research Letters*, *13*(8), 084012. https://doi.org/10.1088/1748-9326/aad400
Willems, P., & Vrac, M. (2011). Statistical precipitation downscaling for small-scale hydrological impact investigations of climate change. *Journal of Hydrology*, *402*(3–4), 193–205. https://doi.org/10.1016/J.JHYDROL.2011.02.030